Checking nonflow assumptions and results via PHENIX published correlations in p+p, p+Au, d+Au, and ^{3}He+Au at $\sqrt{s_{NN}} = 200$ GeV

J. L. Nagle,[1] R. Belmont,[2] S. H. Lim,[3] and B. Seidlitz[1]
[1]*Physics Department, University of Colorado, Boulder, Colorado 80309, USA*
[2]*Physics and Astronomy Department, University of North Carolina, Greensboro, North Carolina 27413, USA*
[3]*Physics Department, Pusan National University, Busan, 46241, South Korea*

(Received 26 July 2021; accepted 31 January 2022; published 14 February 2022)

Recently the PHENIX Collaboration has made available two-particle correlation Fourier coefficients for multiple detector combinations in minimum bias p+p and 0–5% central p+Au, d+Au, and ^{3}He +Au collisions at $\sqrt{s_{NN}} = 200$ GeV [Phys. Rev. C **105**, 024901 (2022)]. Using these coefficients for three sets of two-particle correlations, azimuthal anisotropy coefficients v_2 and v_3 are extracted for midrapidity charged hadrons as a function of transverse momentum. In this paper, we use the available coefficients to explore various nonflow hypotheses as well as to compare the results with theoretical model calculations. The nonflow methods fail basic closure tests with AMPT and PYTHIA/ANGANTYR, particularly when including correlations with particles in the low multiplicity light-projectile going direction. In data, the nonflow adjusted v_2 results are modestly lower in p+Au and the adjusted v_3 results are more significantly higher in p+Au and d+Au. However, the resulting higher values for the ratio v_3/v_2 in p+Au at RHIC compared to p+Pb at the LHC is additional evidence for a significant overcorrection. Incorporating these additional checks, the conclusion that these flow coefficients are dominated by initial geometry coupled with final-state interactions (e.g., hydrodynamic expansion of quark-gluon plasma) remains true, and explanations based solely on initial-state glasma are ruled out. The detailed balance between intrinsic and fluctuation-driven geometry and the exact role of weakly versus strongly coupled prehydrodynamic evolution remains an open question for triangular flow, requiring further theoretical and experimental investigation.

DOI: 10.1103/PhysRevC.105.024906

I. INTRODUCTION

The standard time evolution model for heavy ion collisions involves multiple stages, similar to the stages of the standard big bang time evolution model for the universe. In collisions between large nuclei, for example Au+Au at the Relativistic Heavy Ion Collider (RHIC) and Pb+Pb at the Large Hadron Collider (LHC), the epochs proceed with (i) the initial collision including hard scattering of partons, (ii) a prehydrodynamic phase, (iii) an extended hydrodynamic phase where the matter has a temperature exceeding $T > 155$ MeV and is thus considered a quark-gluon plasma (QGP), and finally after hadronization (iv) a stage of hadronic scattering until the densities are low enough that the particles are free streaming [1]. For more than a decade, the success of hydrodynamics was assumed to imply near-equilibration/thermalization and hence epoch (ii) was referred to as pre-equilibrium. It is now generally recognized that the collision system with rapid longitudinal expansion does not achieve equilibrium [2], and this stage has been renamed prehydrodynamization, viz. the time before hydrodynamics applies—for further discussion, see Refs. [3,4]. Constraining properties of the QGP, such as shear and bulk viscosity and the nuclear equation of state, requires a modeling of all these stages combined with detailed, quantitative comparison with experimental data—see Ref. [5,6] for recent examples.

Similar experimental signatures for QGP formation and the standard time evolution model have also been observed in smaller collision systems such as p+Au, d+Au, ^{3}He +Au at RHIC and p+p, p+Pb at the LHC—see Ref. [7] for a recent review. However, in contrast to the larger QGP droplets formed in $A + A$ collisions, if smaller QGP droplets are indeed formed in smaller collision systems, the time spent in that epoch is significantly shorter, thereby enabling the prehydrodynamic physics to play a larger role. In Ref. [8], the author specifically details how light-heavy ion collisions can provide a window into prehydrodynamic QCD evolution. However, these short-lived systems are also more sensitive to the first stage (i) in terms of both the initial geometry and local (typically few-particle) correlations between particles, the latter of which is often referred to as nonflow.

A specific proposal was put forth to collide proton, deuteron, and helium-3 projectiles on nuclear targets at RHIC, utilizing the unique capabilities of that facility, to discern whether "flow-like" patterns are indeed attributable to mini-QGP droplet formation [9]. The PHENIX Collaboration has published a series of papers culminating in the *Nature Physics* paper with elliptic (v_2) and triangular (v_3) coefficients as a function of transverse momentum (p_T) in p+Au, d+Au, and ^{3}He +Au collisions [10]. Theoretical predictions within the evolution model including a short-lived QGP droplet quantitatively describe the PHENIX data reported in Refs [10,11].

In contrast, a long-standing question of whether initial-state correlations from stage (i) via exotic glasma diagrams could describe the data has been settled. These glasma correlations are not able to describe the magnitudes of v_2 or v_3, nor their p_T dependence, nor the projectile nuclear size dependence [12,13]. However, the influence of other epoch (i) nonflow correlations remains a topic of active discussion.

The PHENIX Collaboration has recently published new results on v_2 and v_3 in p+Au, d+Au, and ^{3}He+Au collisions—in excellent agreement with Ref. [10]—using three sets of two-particle correlations (called the 3×2PC method) [11]. In the 3×2PC method, determination of the v_n requires three sets of two-particle correlations and the extraction of the Fourier coefficients c_n of each set. The publication of the c_n coefficients with statistical uncertainties for all two-particle correlation combinations in Ref. [11] provides ample opportunity for additional exploration of the data and interpretations thereof.

II. NONFLOW SUBTRACTION METHODS

To begin, the individual c_n coeffecients extracted in Ref. [11] determined by performing a Fourier fit to the distribution of angles between pairs of particles, $\Delta\phi$, as

$$C(\Delta\phi) = \sum_n c_n \cos \Delta\phi. \tag{1}$$

These individual coefficients are not necessarily physical quantities on their own, but can be used in combination to extract flow coefficients v_n. For detectors labeled as A, B, and C, the c_n coefficients mathematically represent

$$c_n^{AB} = \langle \cos\left(n(\phi_A - \phi_B)\right)\rangle = \left\langle v_n^A v_n^B \right\rangle, \tag{2}$$

$$c_n^{AC} = \langle \cos\left(n(\phi_A - \phi_C)\right)\rangle = \left\langle v_n^A v_n^C \right\rangle, \tag{3}$$

$$c_n^{BC} = \langle \cos\left(n(\phi_B - \phi_C)\right)\rangle = \left\langle v_n^B v_n^C \right\rangle. \tag{4}$$

The v_n in detector C can then be calculated as

$$v_n^C = \sqrt{\frac{c_n^{AC} c_n^{BC}}{c_n^{AB}}}. \tag{5}$$

In the case of Ref. [11], detector C provides all of the momentum information, so c_n^{AC}, c_n^{BC}, and v_n^C are all determined in the same region of p_T.

We utilize three methods to estimate and subtract nonflow contributions in a given correlation function of interest. These methods assume that the shape the nonflow contribution to the correlation function is multiplicity and collision-system independent. In this study, we use the correlation functions from p+p collisions. The first method, called the c_1 method, estimates the nonflow contributions to c_n coefficients of the correlation function of interest by scaling the c_n coefficients in p+p collisions (c_n^{pp}) by the ratio of c_1 coefficients,

$$c_n^{\text{corrected}} = c_n - c_n^{pp} \frac{c_1}{c_1^{pp}}. \tag{6}$$

This method assumes the c_1 coefficient is purely from nonflow effects, and that there is no flow contribution to the higher coefficients in the low-multiplicity reference, in this case p+p collisions.

We also use a template fit method developed by the ATLAS Collaboration [14]. In the template fit method, a correlation function from high multiplicity $C(\Delta\phi)$ is described by a scaled correlation function from p+p collisions and an additional flow contribution,

$$\begin{aligned} C(\Delta\phi) &= FC^{pp}(\Delta\phi) + C^{\text{flow}}(\Delta\phi) \\ &= FC^{pp}(\Delta\phi) + G\left(1 + \sum_{n=2}^{\infty} 2c_n \cos(n\Delta\phi)\right), \end{aligned} \tag{7}$$

where F and c_n are determined by the fitting procedure, and G is fixed by requiring the integrals of $C(\Delta\phi)$ and $C^{\text{flow}}(\Delta\phi)$ to be equal.

Finally we use the zero-yield-at-minimum (ZYAM) method [15], where one assumes that the number of correlated pairs is zero at the correlation function minimum. This minimum is then subtracted out to obtain the distribution of the correlated per-trigger yields. Application of these correlated per-trigger yields for the nonflow adjustment is detailed in Ref. [16]. In all methods, the extracted c_n coefficients are a multiplication of flow coefficients of two particles, $c_n = v_{n,a} \times v_{n,b}$, which allow for the measurement of the single-particle v_n coefficients with three sets of correlations.

Comparing results between methods is instructive; however, it should be kept in mind that all have a subset of assumptions that are common and thus the range of results is not automatically a good proxy for a systematic uncertainty. More detailed discussion on the nonflow subtraction methods can be found in Ref. [17].

III. DATA RESULTS

The PHENIX detectors utilized in this analysis are the PHENIX Beam-Beam Counter South (BBCS) covering $-3.9 < \eta < -3.1$, the Forward Vertex Tracker South (FVTXS) covering $-2.2 < \eta < -1.2$, the Central Tracker (CNT) covering $-0.35 < \eta < 0.35$, the Forward Vertex Tracker North (FVTXN) covering $1.2 < \eta < 2.2$, and the Beam-Beam Counter North (BBCN) covering $3.1 < \eta < 3.9$. The kinematic selections are shown in Fig. 1, reproduced from Ref. [11].

We note that, in all plots in this paper, the v_2 and v_3 values labeled as PHENIX data are calculated using Eq. (5) and the Fourier coefficients c_2 and c_3 of the three two-particle correlations given by PHENIX in Ref. [11]. Figure 2 shows as closed points the PHENIX experimental results for v_2 (top) and v_3 (bottom) as a function of p_T at midrapidity for p+Au (left), d+Au (middle), and ^{3}He+Au (right) central 0–5% collisions at $\sqrt{s_{NN}} = 200$ GeV. These results are extracted via three sets of two-particle correlations—between the BBCS-FVTXS, BBCS-CNT, and FVTXS-CNT—and thus labeled as BBCS-FVTXS-CNT. This combination was chosen since it has the largest rapidity gaps between detectors and the BBCS and FVTXS, being in the Au-going direction, which have the highest multiplicities thus minimizing nonflow contributions. The uncertainties for the 3×2PC results are statistical only.

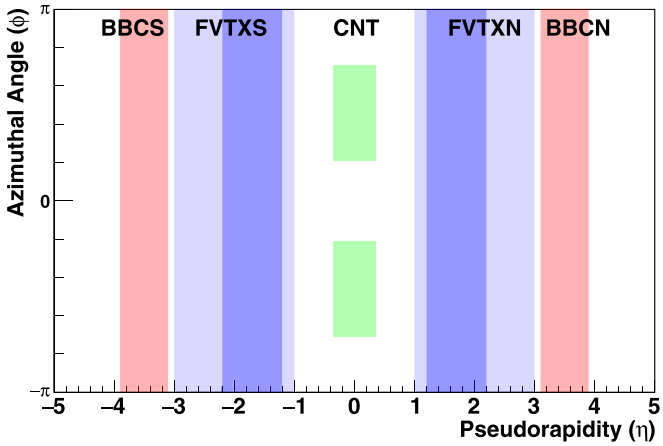

FIG. 1. Azimuthal (ϕ) and pseudorapidity (η) acceptance of various PHENIX detector subsystems. Reproduced from Ref. [11].

The PHENIX experiment estimated nonflow contributions in the earlier event plane analysis and included them as asymmetric systematic uncertainties [10]. However this systematic uncertainty was only determined in the event plane method from the BBCS-CNT correlation—see Ref. [10] for details. We overlay those systematic uncertainties for the p+Au v_2 and v_3 example for visual comparison purposes, noting that the p_T binning is slightly different from the 3×2PC results. It is only with the new analysis via 3×2PC [11] that one can apply the nonflow method to all contributions as detailed below.

Figure 2 also shows as open points the adjusted results when applying the template fit method, as detailed above. The low multiplicity reference comes from the PHENIX p+p minimum bias data, which corresponds to 55±5% of the inelastic cross section of 42 mb [18]. The template fit method is applied individually to each of the three sets of two-particle correlations.

As the c_2 coefficients are positive in p+p, the adjusted $p/d/^3$He +Au c_2 coefficients decrease. However, in calculating the v_2, two correlation coefficients are in the numerator and one in the denominator, and hence the direction of the adjustment to v_2 is nontrivial. In contrast, the c_3 coefficients are negative in p+p, and hence the adjusted $p/d/^3$He +Au c_3 coefficients increase. For the same reason as for v_2, the direction of the adjustment to v_3 is nontrivial. In the end, however, the v_2 (v_3) values decrease (increase) in all cases, in line with expectations. The gray bands indicate the statistical uncertainties only on the template-adjusted values resulting from the statistical uncertainties on the coefficients in $p/d/^3$He +Au and the p+p reference. There are some cases where the combination of c_n coefficients results in an imaginary v_n, and these are plotted as negative values on the vertical scale. The solid (dashed) lines are fits to the ^{3}He +Au raw (template-adjusted) results and are shown in all panels for comparison.

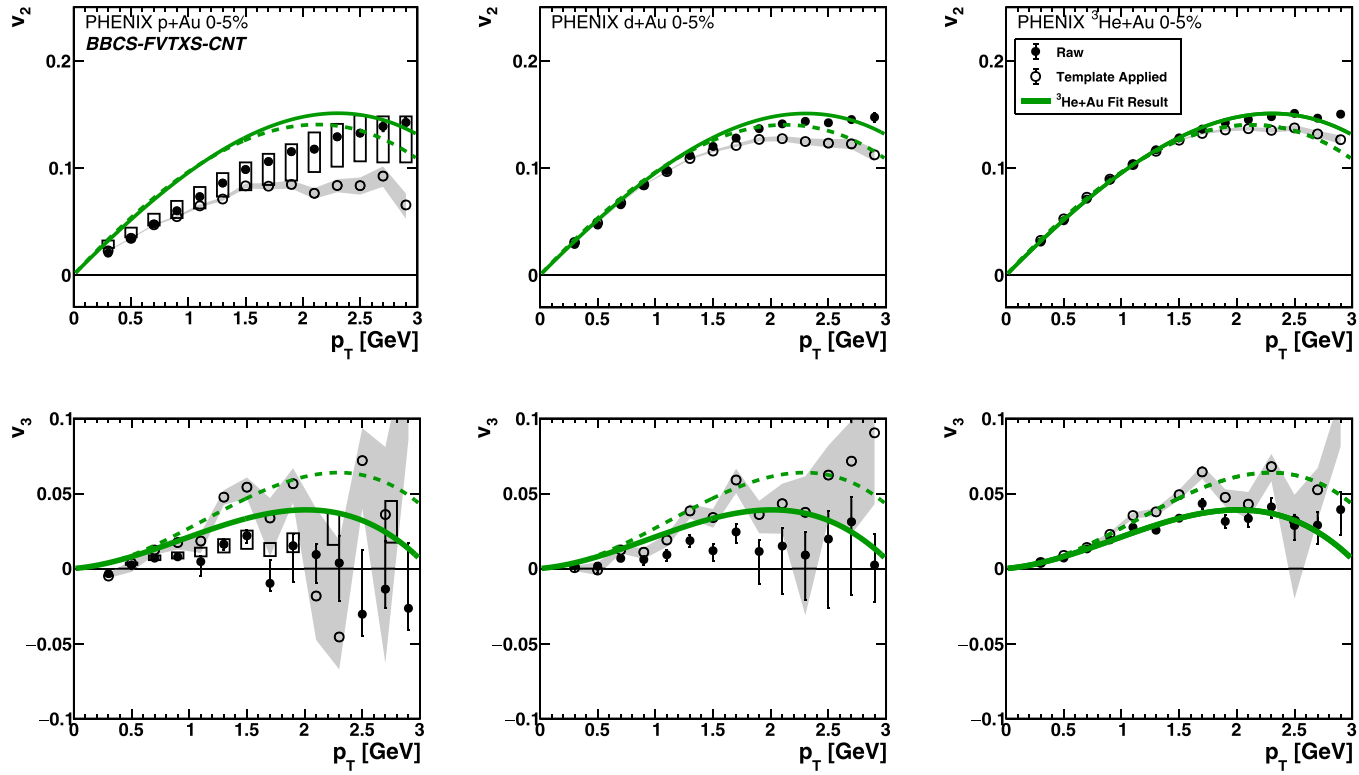

FIG. 2. PHENIX published v_2 (top) and v_3 (bottom) for p+Au, d+Au, and ^{3}He +Au 0–5% collisions at $\sqrt{s_{NN}} = 200$ GeV from left to right, respectively. Solid points are the raw values and the open points are template adjusted. Nonflow systematic uncertainties estimated by the PHENIX Collaboration in Ref. [10] are shown for p+Au v_2 and v_3 results as examples. The solid and dashed lines are fits to the ^{3}He +Au results. The points shown are extracted via Eq. (5) using the published PHENIX Fourier coefficients of the three two-particle correlations in Ref. [11].

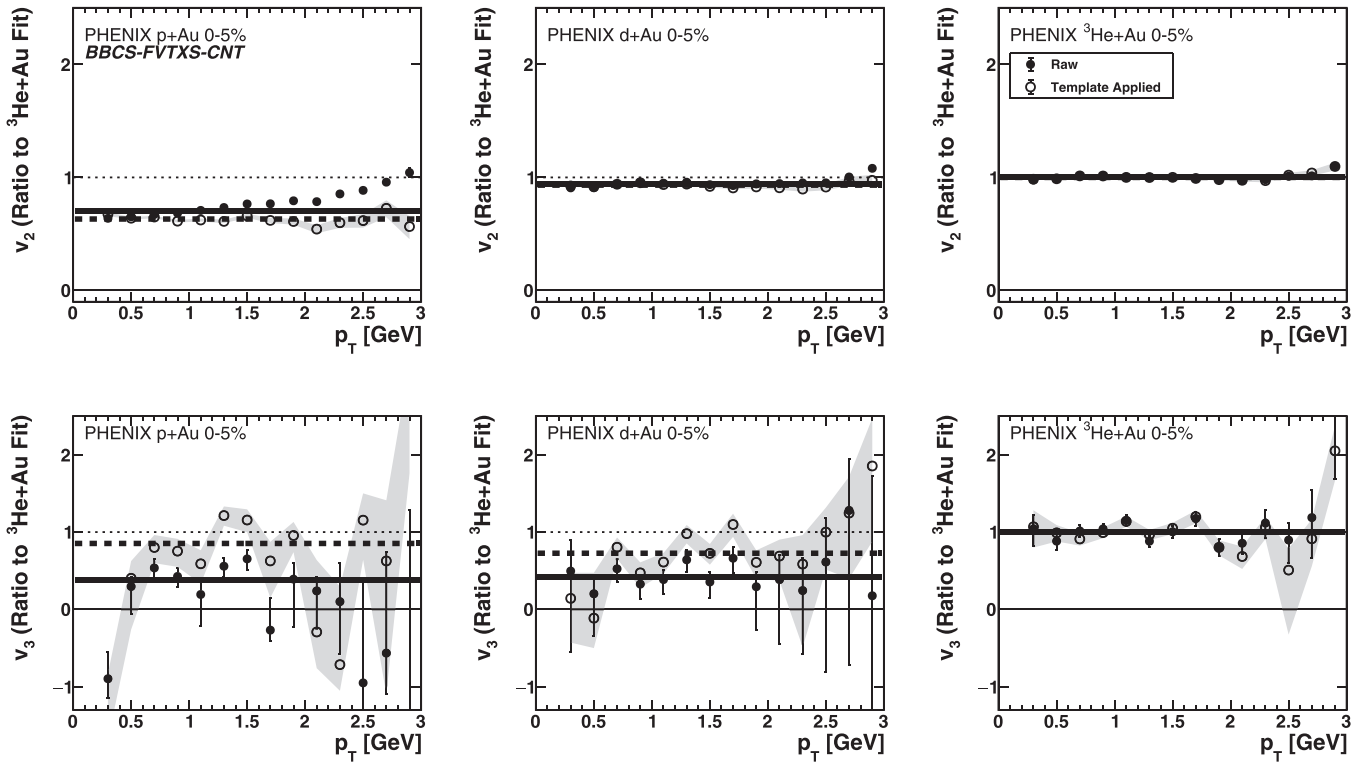

FIG. 3. PHENIX published v_2 (top) and v_3 (bottom) for p+Au, d+Au, and ^{3}He +Au 0–5% collisions at $\sqrt{s_{NN}} = 200$ GeV from left to right, respectively, as a ratio to the ^{3}He +Au fit functions. Solid points are the raw values and the open points are template adjusted. Simple horizontal level fits are shown as solid and dashed lines for the two cases, respectively. The values of v_2 and v_3 used to calculate these ratios are extracted via Eq. (5) using the published PHENIX Fourier coefficients of the three two-particle correlations in Ref. [11].

The template-adjusted p+Au results are consistent with the raw results within the original non-flow estimated uncertainty for p_T <2 GeV. The template-adjusted results for the v_3 are higher than the raw v_3 beyond the original nonflow estimated uncertainties.

Figure 3 shows the ratio of the points from Fig. 2 relative to the ^{3}He +Au fits, and hence by construction the rightmost panel values are consistent with one. One observes a slightly lower v_2 in d+Au relative to ^{3}He +Au, of order 5–10%, and independent of p_T regardless of the template adjustment. The v_2 in p+Au relative to ^{3}He +Au is slightly lower with the template adjustment and appears to remove the p_T dependence above 2 GeV seen in the raw results. For the v_3, the p+Au and d+Au raw results are consistently 60% lower than the ^{3}He +Au and flat with p_T within uncertainties. The template-adjusted results are higher and more consistent with only 15–30% lower than the ^{3}He +Au results. As before, the gray bands are propagated statistical uncertainties only.

Figures 4 and 5 show the $v_{2,3}$ and ratios to the ^{3}He +Au fits but now for two additional sets of detector combinations (FVTXS-CNT-FVTXN and BBCS-CNT-FVTXN). The nonflow contributions are expected to be larger in the FVTXN due to the significantly lower multiplicity in the light-projectile-going direction and the lower expected flow—see Ref. [19], for example. The raw v_2 results from both new combinations are higher than the BBCS-FVTXS-CNT combination discussed previously, most strikingly so in the p+Au case. The template-adjusted results for different detector combinations are in better agreement with each other, though a 15–25% relative difference remains in the p+Au case.

In the v_3 case, the combinations involving the FVTXN result in imaginary raw v_3 values in p+Au and d+Au, plotted as negative values for visualization. The template-adjusted values shift significantly upward into the positive, real range for many data points; however, the three detector combinations of values remain disparate in the p+Au and d+Au cases.

We also show the three detector combinations and the c_1-method adjustment in Figs. 6 and 7. The results are qualitatively similar to the template method. However, the adjustment is somewhat larger, as can be seen in the p+Au v_2 values, which are now slightly below the systematic uncertainties of the PHENIX data even for $p_T < 2$ GeV. Since the c_1 method assumes no flow in the p+p reference, this larger nonflow adjustment is in line with expectations. Results with the ZYAM method (not shown) are qualitatively similar to the template and c_1-method adjustments.

IV. NONFLOW CHECKS

One method to check the nonflow adjustment methods is with Monte Carlo calculations. Applications of the methods to Monte Carlo calculations without final-state interactions, i.e., flow, have been done with PYTHIA, PYTHIA/ANGANTYR, HIJING, and AMPT, which also includes final-state partonic and hadronic scattering—see Ref. [17] for example. Here we

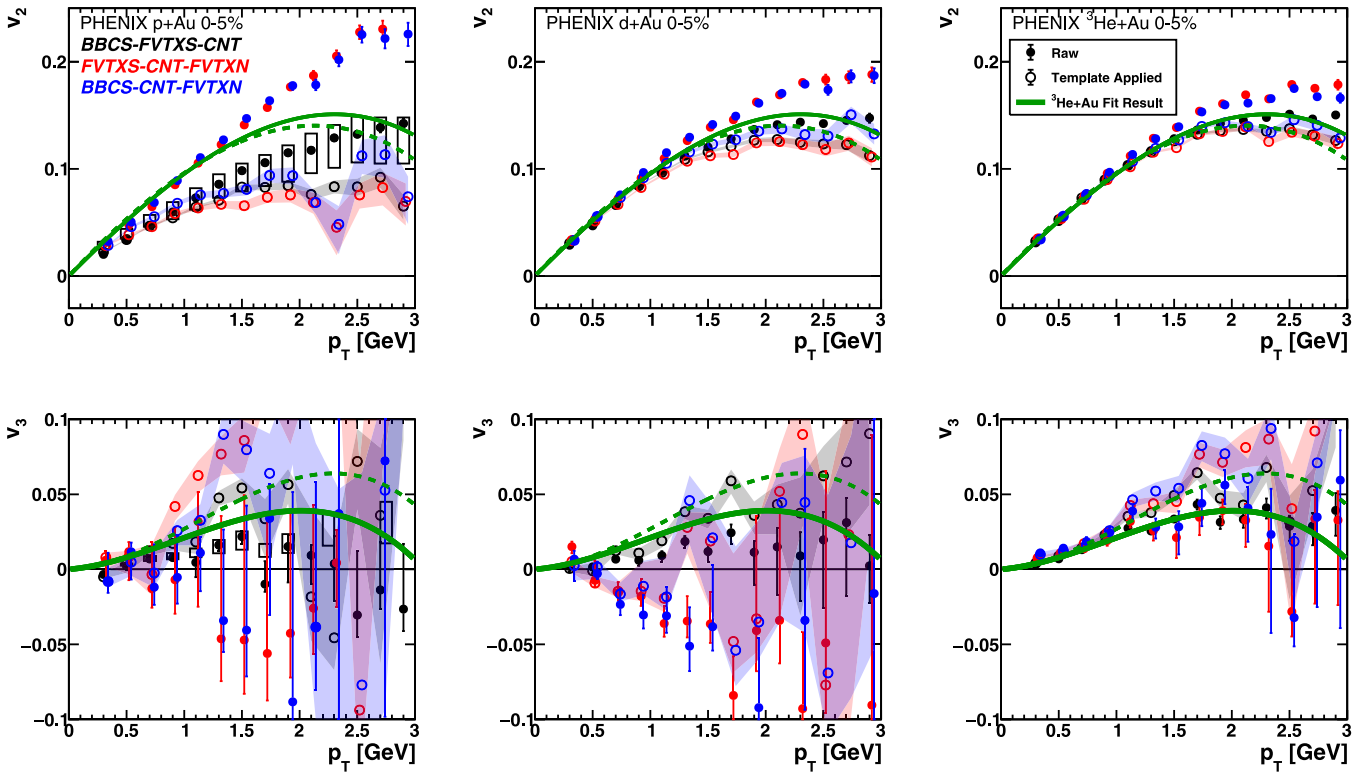

FIG. 4. PHENIX published v_2 (top) and v_3 (bottom) for p+Au, d+Au, and ^{3}He +Au 0–5% collisions at $\sqrt{s_{NN}} = 200$ GeV from left to right, respectively, from three different sets of detector combinations. Solid points are the raw values and the open points are template adjusted. Nonflow systematic uncertainties estimated by the PHENIX Collaboration in Ref. [10] are shown for p+Au v_2 and v_3 results as an example. The solid and dashed lines are fits to the ^{3}He +Au results. The points shown are extracted via Eq. (5) using the published PHENIX Fourier coefficients of the three two-particle correlations in Ref. [11].

utilize two of these calculations to test the nonflow adjustment methods utilizing the PHENIX kinematic selections.

A Multi-Phase Transport (AMPT) is a nonhydrodynamic framework for calculating the various epochs in the heavy ion time evolution [20]. For the initial stage (i) the geometry and initial color strings come from the HIJING model, the next stage (ii) is essentially free streaming modeled by a formation time for the partons, (iii) is modeled via on-shell parton scattering in the ZPC framework, and (iv) is modeled with the ARC hadron scattering package. We have run 100 million minimum bias p+p and central (impact parameter $b < 2$ fm) p+Au events and analyzed the Monte Carlo data via the same sets of three detector combinations (in terms of p_T and pseudorapidity coverage) as used in the PHENIX analysis. The results of using the correlation coefficients to calculate the raw v_n and the template-method adjusted v_n are shown in Fig. 8.

Similar to the PHENIX data, the raw AMPT v_2 values are significantly higher with the FVTXS-CNT-FVTXN and BBCS-CNT-FVTXN combinations, presumably due to larger nonflow contributions; however, all the v_2 values are almost a factor of two higher than the PHENIX data. In the case of v_3, the BBCS-FVTXS-CNT result is near zero, while the other combinations yield imaginary results (shown as negative values). Also shown are the template-adjusted values, which have significant variations between detector combinations for both v_2 and v_3. The large imaginary result in the BBCS-CNT-FVTXN combination results from the c_n sign in the BBCS-FVTXN combination. The solid dashed lines are the "truth" result calculated as the hadron v_n relative to the Ψ_n defined from the initial parton geometry—see Ref. [21] for details on the method. We highlight that this method may not correspond to the absolute truth expectation even if nonflow is perfectly accounted for. In particular, the truth calculation yields the average v_n, while the result from the two-particle correlation method is essentially $\sqrt{v_n^2}$. We have estimated the effect from this definitional difference via the geometry distribution and it results in a truth v_n that may be 20% underestimated. Additionally, the final state hadron flow may have additional fluctuations beyond those from the geometry. Even with these caveats, it is clear from the disagreement between kinematic combination results, the imaginary values, etc., that the AMPT results do not show good closure, i.e., a validation of the methodology. The c_1 and ZYAM methods yield qualitatively similar conclusions.

The failure of the nonflow adjustment methods is not unexpected in the AMPT case. First, from tracing the parton scattering history, the hard scattered partons do scatter further with medium partons. This means that the "jet shape" explicitly changes between p+p and p+Au collisions, and thus violates one of the basic assumptions in all of the nonflow methods [22]. This feature is directly observed by tracing partons from hard scattering in the AMPT initial stage, modeling via HIJING, and counting their subsequent scattering with soft partons in the medium. Additionally, the HIJING modeling

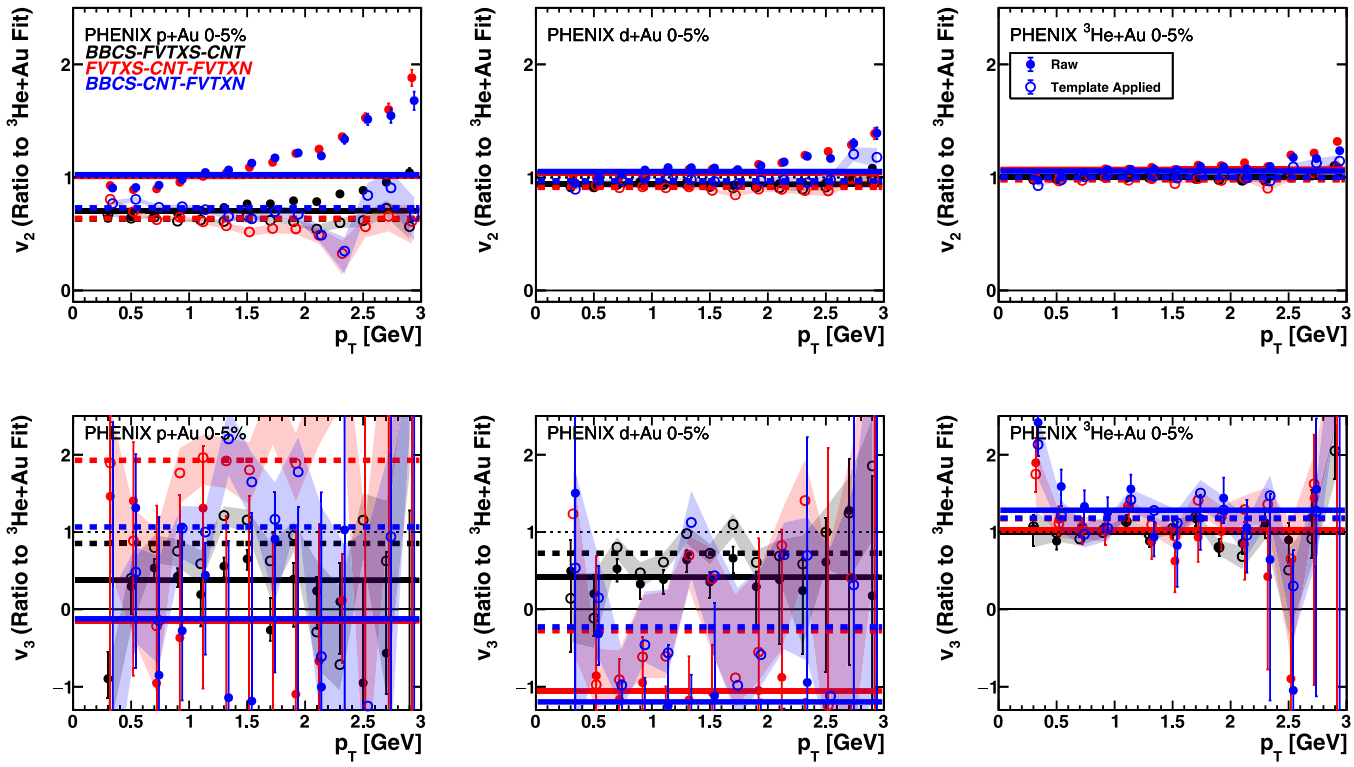

FIG. 5. PHENIX published v_2 (top) and v_3 (bottom) for p+Au, d+Au, and ^{3}He +Au 0–5% collisions at $\sqrt{s_{NN}} = 200$ GeV from left to right, respectively, as a ratio to the ^{3}He +Au fit functions, from three difference sets of detector combinations. Solid points are the raw values and the open points are template adjusted. Simple horizontal level fits are shown as solid and dashed lines for the two cases, respectively. The values of v_2 and v_3 used to calculate these ratios are extracted via Eq. (5) using the published PHENIX Fourier coefficients of the three two-particle correlations in Ref. [11].

of this initial stage results in a near-side jet correlation that has been observed to be wider than in real p+p data. This additional nonflow contribution has been demonstrated to lead to adjustment failures [17].

Next we check the methods with the PYTHIA/ANGANTYR Monte Carlo [23]. The results are shown in Fig. 9, and indicate a large nonflow contribution with the largest for detector combinations including the FVTXN. The v_3 coefficients are imaginary in all cases. The nonflow adjusted results show a significant overcorrection in the case of the FVTXN detector combinations. Results from the combination with the smallest nonflow (BBCS-FVTXS-CNT) have adjusted results reasonably close to zero, though still with a residual nonclosure (i.e., a nonzero extraction of final-state v_n). The c_1 and ZYAM methods yield qualitatively similar conclusions.

V. DISCUSSION

The above calculations are mathematically well defined. The question is whether the raw results or the various nonflow adjusted results are reliable in a way that experiments can define "experimental quantities" with well-constrained uncertainties. One clear takeaway message is that the assumptions of the nonflow methods are always violated, and the questions are how much are they violated and how big is the correction relative to these problems [17].

In the case of v_2 for the p+Au, d+Au, and ^{3}He +Au systems, the template, c_1 method, and ZYAM adjustments yield reasonable (10–25% level) agreement between detector combinations. The p+Au results are reasonably consistent with the raw results with asymmetric nonflow systematic uncertainties up to $p_T = 2$ GeV. The nonflow adjustment is particularly prone to over-correction at higher p_T as demonstrated above.

However, the v_3 results in p+Au and d+Au are almost a factor of two higher relative to ^{3}He +Au in the template, c_1 method, and ZYAM adjusted cases compared with the raw case for the BBCS-FVTXS-CNT detector combination. These differences are larger than the PHENIX published nonflow asymmetric systematic uncertainty [10]. For the other two detector combinations, the v_3 is imaginary for the raw values and receives a very large adjustment from the nonflow methods and with very large statistical uncertainties.

Focusing on the case with the smallest nonflow contributions, Fig. 10 shows the PHENIX raw data and template-adjusted data for v_2 and v_3 in the three collisions systems, p+Au, d+Au, and ^{3}He +Au for the BBCS-FVTXS-CNT detector combination. In the upper panel, overlaid are calculations from the authors MSTV in the initial-state glasma framework [12,13]. The calculations fail to describe the data with or without the nonflow adjustment. In the lower panel, overlaid are hydrodynamic calculations

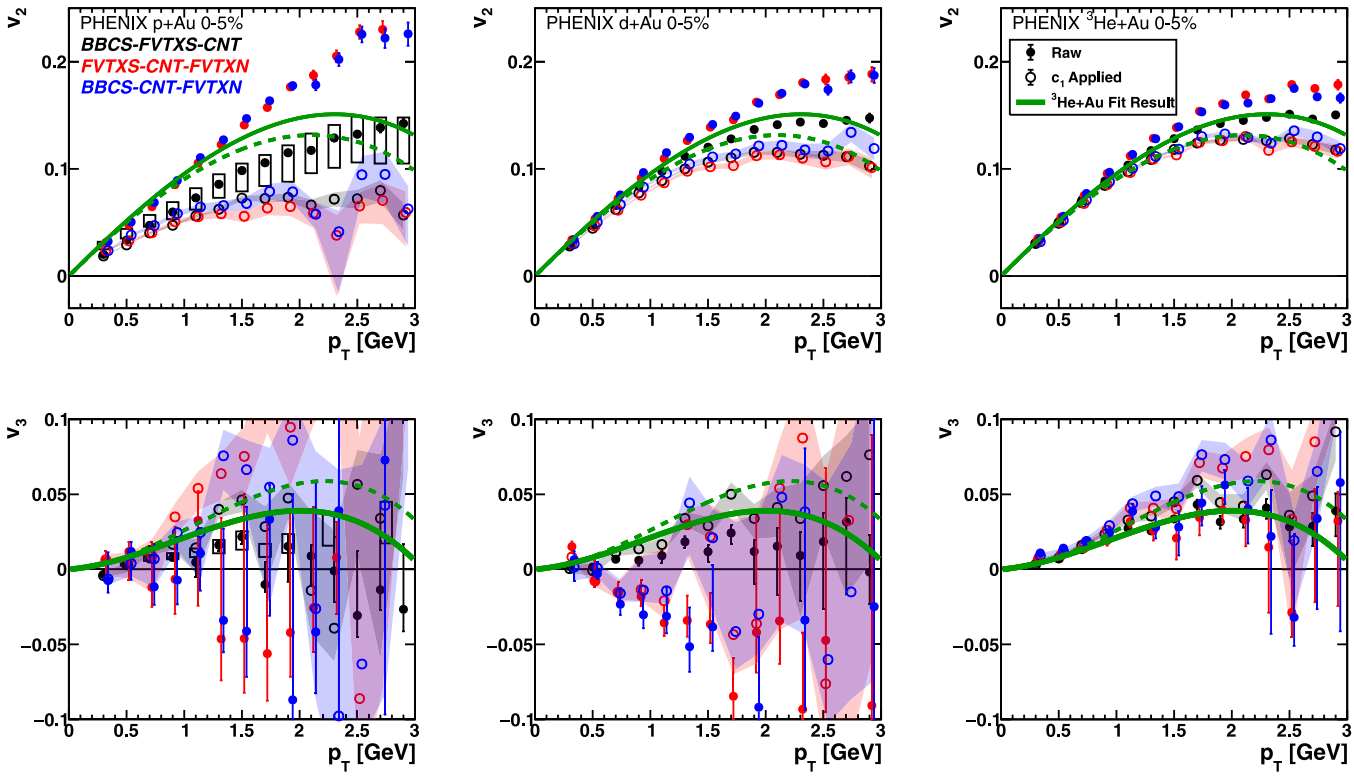

FIG. 6. PHENIX published v_2 (top) and v_3 (bottom) for p+Au, d+Au, and ^{3}He +Au 0–5% collisions at $\sqrt{s_{NN}} = 200$ GeV from left to right, respectively. Solid points are the raw values and the open points are c_1-method adjusted. Nonflow systematic uncertainties estimated by the PHENIX Collaboration in Ref. [10] are shown for p+Au v_2 and v_3 results as examples. The solid and dashed lines are fits to the ^{3}He +Au results. The points shown are extracted via Eq. (5) using the published PHENIX Fourier coefficients of the three two-particle correlations in Ref. [11].

with the SONIC (no pre-flow) and SUPERSONIC (with strong pre-flow) models [8] and the IP-GLASMA+MUSIC+URQMD model [24]. As an aside, there are significantly larger theoretical uncertainties in the IP-GLASMA+MUSIC+URQMD [24] case due to various choices in matching conditions between the weakly coupled pre-hydrodynamic (IP-GLAMSA) and hydrodynamic (MUSIC) stages, which does not exist in SUPERSONIC where both stages are strongly coupled. With or without nonflow adjustment, the v_2 ordering between $p/d/^3$He +Au systems follows expectations from initial geometry differences and final-state interactions. The v_3 is lower in p+Au and d+Au compared with ^{3}He +Au, but the degree depends highly on the treatment of nonflow. Hence, the conclusions regarding the general agreement with geometry ordering and hydrodynamic modeling and the ruling out of initial-stage glasma correlations are retained.

Despite the general agreement with hydrodynamic calculations, there are important physics implications for the variation in v_3 in p+Au and d+Au collisions. One important open issue in the field is the nature of the initial geometry in small systems. Is this dictated by color strings? Do multiparton interactions play a role? Are there simply three or four or five clustered constituents to the nucleon? Are there substantial contributions from the fluctuations in entropy deposition per constituent-constituent collision? As shown in the PHENIX publication [11], reproduced here as Table I, the initial geometry of the collision systems has significant variation depending on the modeling of the aforementioned effects. The template-, c_1-, and ZYAM-adjusted values show a larger system-geometry difference in v_2 and a smaller system-geometry difference in v_3 compared to the raw results. Thus, the v_2 (v_3) adjusted values might indicate a smaller (larger) relative role for fluctuation-driven (particle production, nucleonic, subnucleonic) versus intrinsic geometry.

Another key effect is the physics of the prehydrodynamic stage (ii)—see the calculation differences between SONIC without pre-flow and SUPERSONIC with strong preflow in Fig. 10.

One can partially isolate this effect by comparing p+Au collisions at RHIC and p+Pb collisions at the LHC. If one makes the assumption that the initial geometry is very similar at both collision energies, the relative triangularity and ellipticity should be the same. Simple Monte Carlo Glauber calculations, where the only differences in geometry arise from Au versus Pb nuclei and the difference in inelastic N-N cross sections, yield values for ε_2, ε_3 that are only 5–10% larger in p+Au compared to p+Pb and only a few percent different in the ratio $\varepsilon_3/\varepsilon_2$. Figure 11 shows various hydrodynamic and transport model calculations and the predicted double ratio of v_3/v_2 in p+Au collisions at $\sqrt{s_{NN}} = 200$ GeV and p+Pb collisions at $\sqrt{s_{NN}} = 5$ TeV. All of the results for the double ratio are significantly below one, except for the IP-GLASMA+MUSIC+URQMD calculation [24], which is close to

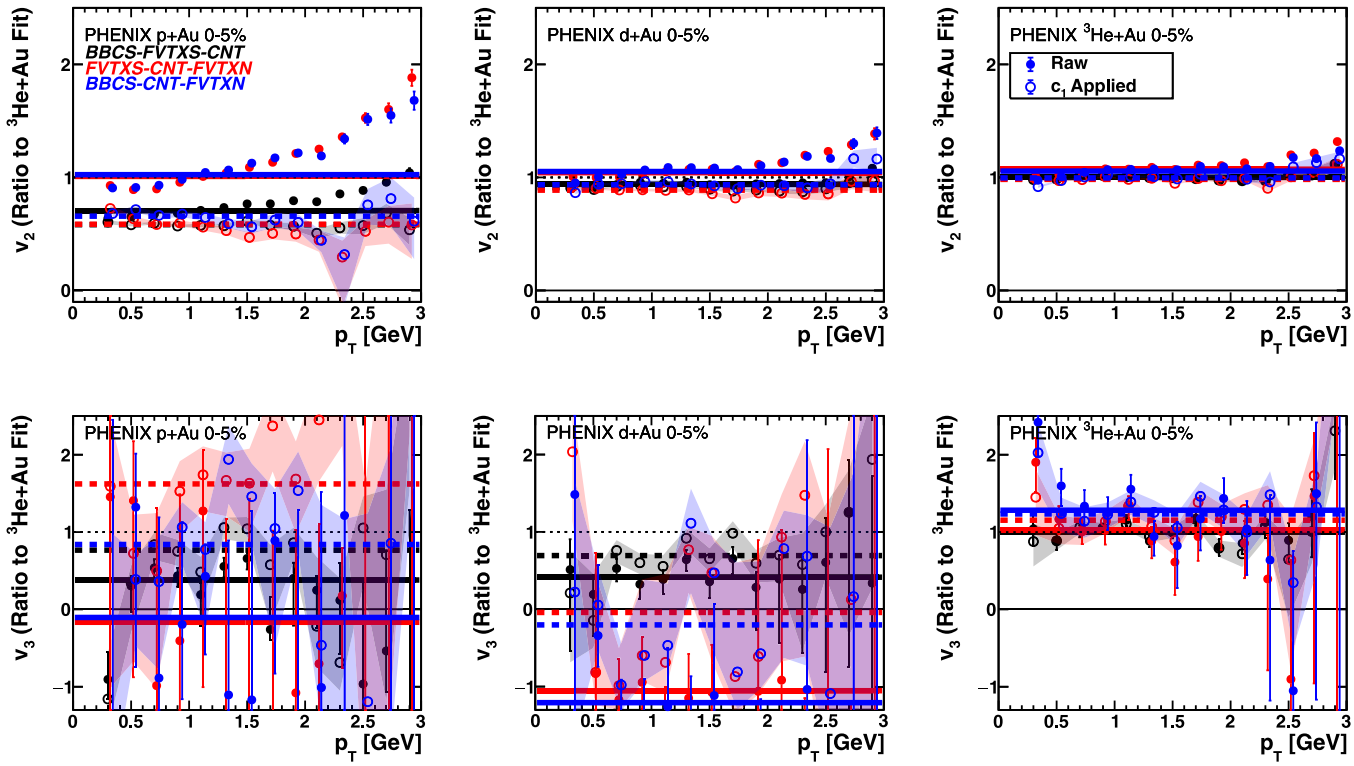

FIG. 7. PHENIX published v_2 (top) and v_3 (bottom) for p+Au, d+Au, and ^{3}He +Au 0–5% collisions at $\sqrt{s_{NN}} = 200$ GeV from left to right, respectively, as a ratio to the ^{3}He +Au fit functions. Solid points are the raw values and the open points are c_1-method adjusted. The values of v_2 and v_3 used to calculate these ratios are extracted via Eq. (5) using the published PHENIX Fourier coefficients of the three two-particle correlations in Ref. [11].

one. The IP-GLASMA matching conditions to hydrodynamics or initial geometry between the collision energies may differ, though that needs to be confirmed.

The reason for values near or significantly below one is that the smaller scale features of higher geometric moments (ε_n) take more time in the hydrodynamic stage to translate into flow moments v_n. Hence the lower multiplicity, lower initial temperature hydrodynamic stage in collisions of lower energy at RHIC correlates with a shorter lifetime hydrodynamic stage and thus a more striking decrease in v_3 relative to v_2. The very low double ratio (0.4–0.5) in the SONIC without preflow and fixed $\eta/s = 0.08$ and the much higher SUPERSONIC result (0.6–0.7) with preflow (modeled via AdS/CFT in the strongly coupled limit) is notable [8]. With a short hydrodynamic lifetime, particularly at RHIC, the additional push of the strongly coupled preflow stage adds significantly to the translation of geometry to flow. The calculation directly from Ref. [8] without preflow has an $\eta/s = 0.08$ at RHIC and $\eta/s = 0.16$ at the LHC—and this compensates to bring the double ratio up, though still significantly below one. Calculations within the AMPT framework also yield a result significantly below one.

One can make the same type of comparison between LHC p+Pb and RHIC p+Au collisions with experimental data. Figure 12 (upper) shows the ATLAS published p+Pb at $\sqrt{s_{NN}} = 5$ TeV data ratio for v_3/v_2 as a function of p_T. The dashed line is a fit to the data. The PHENIX p+Au raw results from BBCS-FVTXS-CNT with statistical uncertainties only are shown, along with the template-adjusted values. The raw p+Au results are lower by a factor of 2–3 compared to the ATLAS p+Pb values. Figure 12 (lower) shows the ratio of PHENIX data to the ATLAS data fit compared with theoretical calculations. The PHENIX raw data ratios are qualitatively consistent with the SONIC calculations without preflow, which was utilized in the original $p/d/^3$He +Au proposal paper [9], though drop significantly at the highest p_T. For the template-adjusted values for $p_T > 1.2$ GeV, the results are significantly higher than the ATLAS p+Pb values (a factor of 1.5–2). For $p_T < 1.2$ GeV, the PHENIX template-adjusted values are reasonably consistent with the ATLAS p+Pb result, i.e., a double ratio near one.

It is highly probable, though not definitive, that the nonflow adjusted values are too low for v_2 and too high for v_3, i.e., an overcorrection. Without Monte Carlo with comparable flow and nonflow contributions to real data, it is a challenge to further pin down the range of v_3 values reliably. Thus, the issues of whether strong preflow in stage (ii) is needed and/or the intrinsic geometry relative to fluctuation-driven geometry is in a different balance for triangularity are still open.

VI. COLLAPSE OF TRIANGULAR FLOW

Within the (SUPER)SONIC framework, triangular flow v_3 essentially collapses in p+A collisions below a particular collision energy [8]. In the calculation, as the collision energy is reduced, what is really changing is the matching to the final

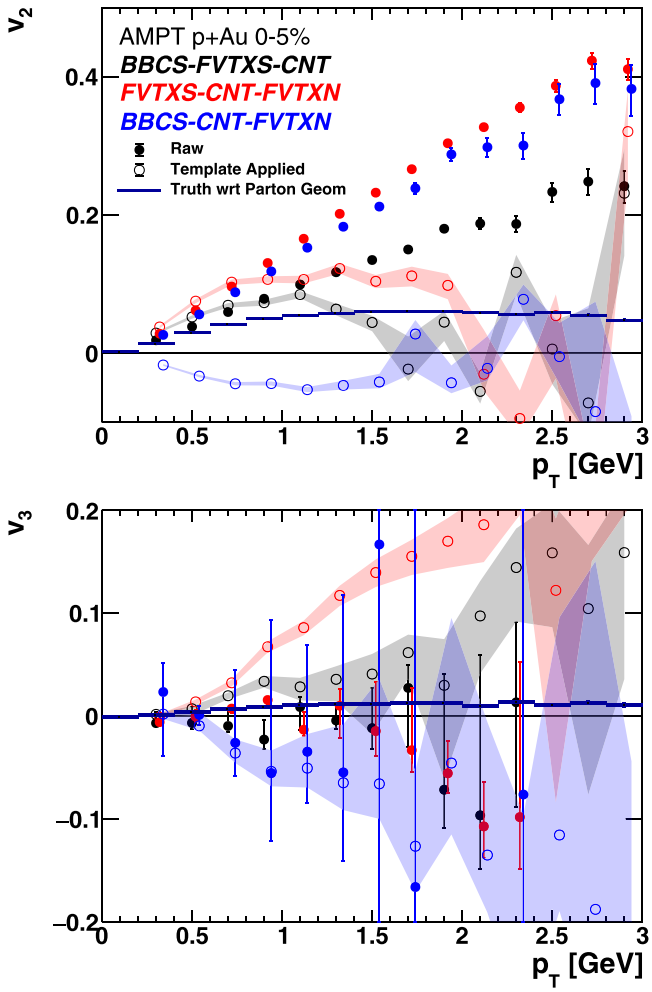

FIG. 8. AMPT v_2 (top) and v_3 (bottom) for p+Au central ($b < 2$ fm) collisions at $\sqrt{s_{NN}} = 200$ GeV from from three different sets of detector combinations. Solid points are the raw values and the open points are the template-adjusted values. The solid horizontal lines correspond to the "truth" result, i.e., with respect to the parton geometry, as detailed in the text. Negative values correspond to imaginary results when one or more of the coefficients in the square root are negative.

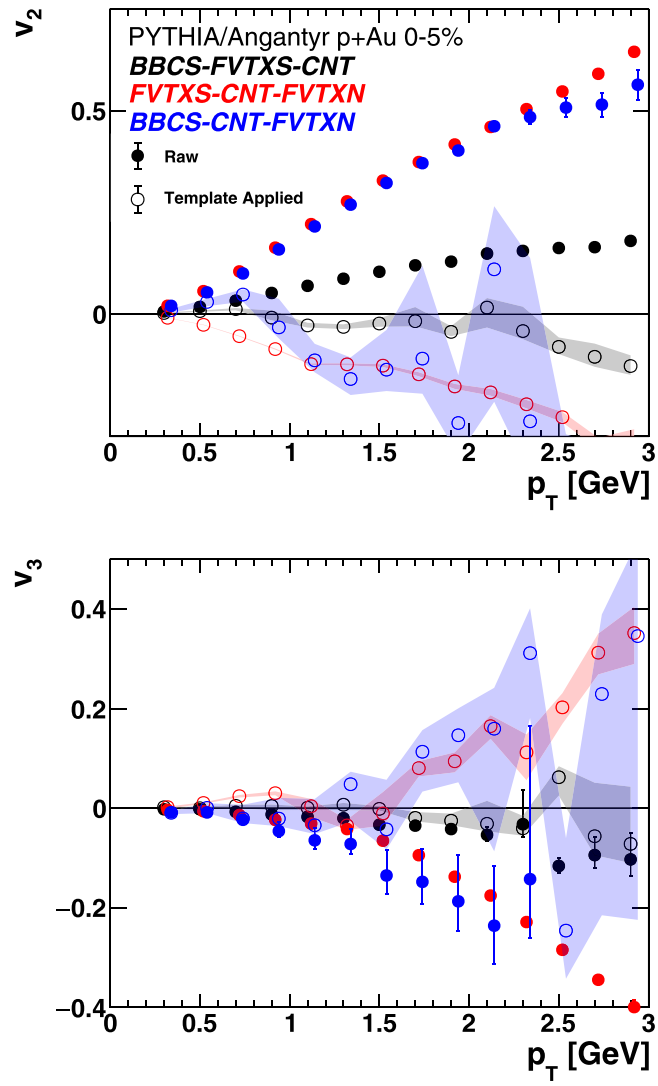

FIG. 9. PYTHIA/ANGANTYR v_2 (top) and v_3 (bottom) for p+Au central ($b < 2$ fm) collisions at $\sqrt{s_{NN}} = 200$ GeV from from three different sets of detector combinations. Solid points are the raw values and the open points the template-adjusted values. Negative values correspond to imaginary results when one or more of the coefficients in the square-root are negative.

hadron $dN_{ch}/d\eta$, which effectively shrinks the initial entropy and the length of time in the hydrodynamic phase, i.e., the lifetime of the QGP. One can construct a map from $dN_{ch}/d\eta$ to v_3/v_2. Since SUPERSONIC is 2+1D hydrodynamics, each collision energy is simply treated as a slice in pseudorapidity. Thus, we have generated a map between collision energies and pseudorapidity in p+Au collisions at $\sqrt{s_{NN}} = 200$ GeV.

Shown in Fig. 13 is the pseudorapidity distribution $dN_{ch}/d\eta$ from AMPT in minimum-bias p+p (with and without final-state interactions) and central ($b < 2$ fm) p+Au, d+Au, and ^{3}He +Au collisions at $\sqrt{s_{NN}} = 200$ GeV. The approximate pseudorapidity acceptances for the PHENIX detector systems are marked with boxes. Within the pseudorapidity range of the PHENIX measurement of $dN_{ch}/d\eta$ in these systems [19], AMPT is in reasonable agreement with data.

The (SUPER)SONIC results (with and without strongly coupled preflow) in p+A collisions as a function of $\sqrt{s_{NN}}$ are given in Ref. [8], including values of $dN_{ch}/d\eta$. Using the AMPT distribution of $dN_{ch}/d\eta(\eta)$, we have calculated the ratio v_3/v_2 as a function of pseudorapidity in p+Au collisions at 200 GeV. The resulting predictions are shown in Fig. 14. There is a precipitous drop in the ratio when transitioning to forward pseudorapidity without pre-flow, which is expected from the same drop seen from (SUPER)SONIC in going from p+Au at 200 to 62.4 GeV—see Fig. 4 from Ref. [8]. The addition of strongly coupled preflow mitigates this drop, though the ratio does decrease as the lifetime of the whole medium evolution shrinks in the forward rapidity slices. These calculations put a spotlight on the important role of prehydrodynamic evolution and the importance in treating these asymmetric

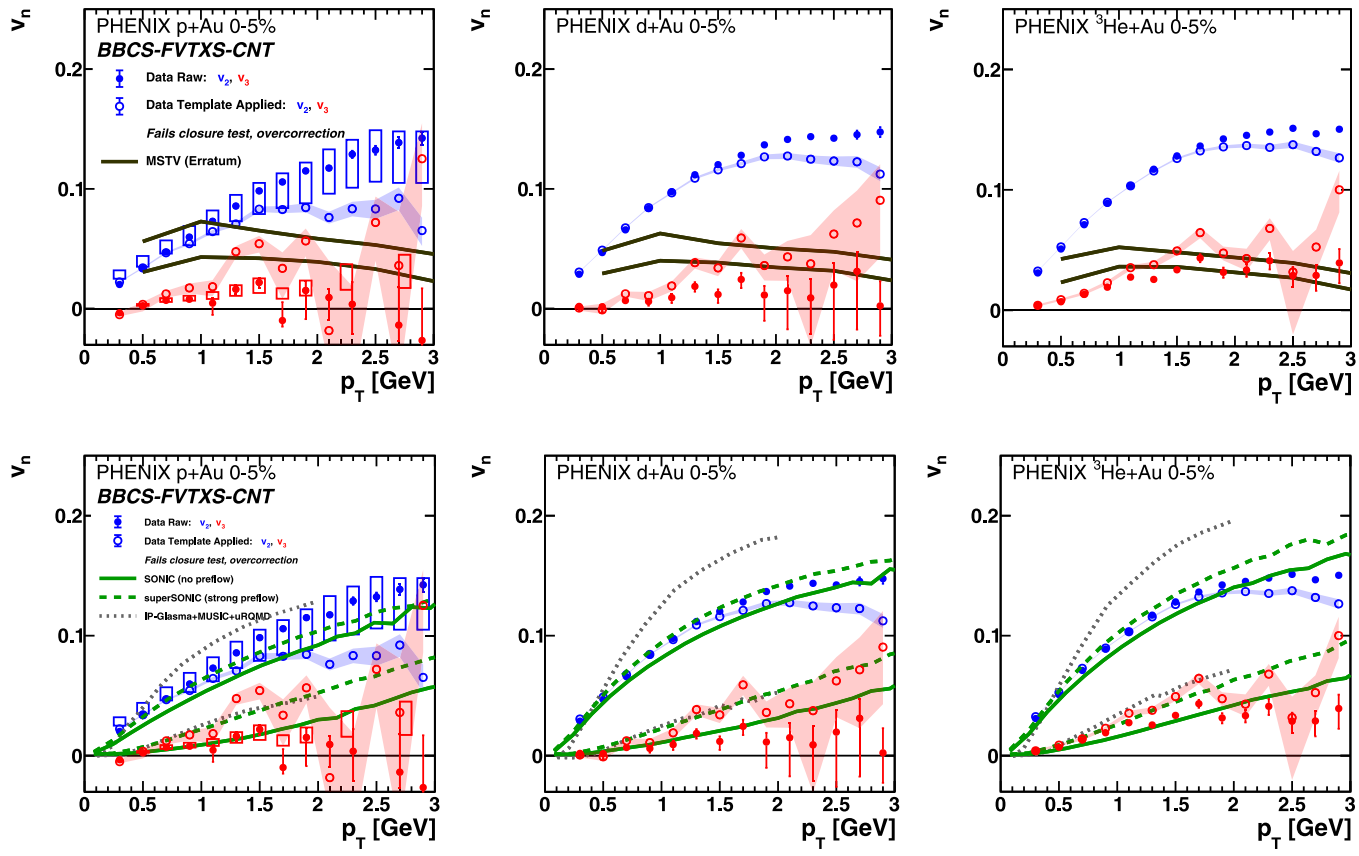

FIG. 10. PHENIX raw and template correction applied data v_2 and v_3 as a function of p_T in central p+Au, d+Au, and ^{3}He +Au collisions. Also shown are theoretical calculations (initial-state glasma results in the upper panels and final-state hydrodynamic results in the lower panels) detailed in the text. The calculations are taken directly from the references: MSTV [12,13], SONIC and SUPERSONIC [8], and IP-GLASMA+MUSIC+URQMD [24].

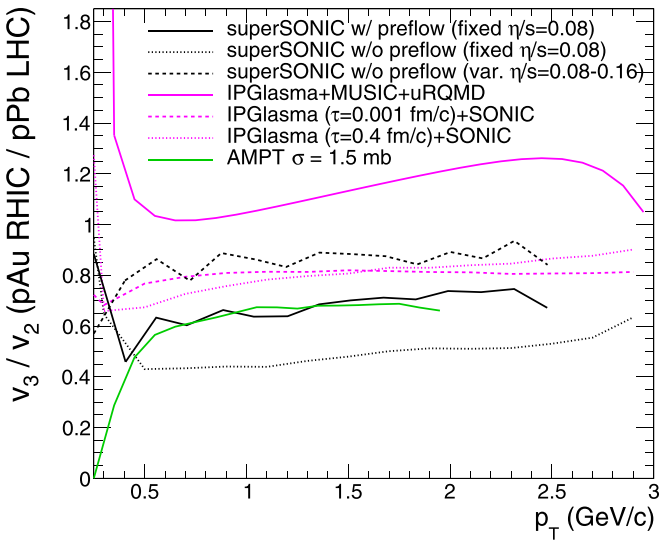

FIG. 11. Various hydrodynamic and parton transport calculations with different initial states, pre-hydrodynamic modeling, and hydrodynamic evolution with results for the double ratio of v_3/v_2 in p+Au collisions at $\sqrt{s_{NN}} = 200$ GeV over v_3/v_2 in p+Pb collisions at $\sqrt{s_{NN}} = 5$ TeV. See text for details.

collisions systems asymmetrically, i.e., not assuming any symmetry even near midrapidity. The calculations also highlight that nonflow effects, which are largest when $dN_{ch}/d\eta$ is smallest and when the real flow coefficient is smallest, could be highly pseudorapidity dependent. A future experimental measurement of the v_3/v_2 ratio over a broad pseudorapidity range, though challenging, would be most instructive.

VII. LONGITUDINAL DECORRELATIONS

So far we have focused on flow and nonflow contributions, but longitudinal decorrelations may also play a significant role. If the entropy deposition in the transverse plane is dependent on the longitudinal or pseudorapidity slice, then the magnitude and orientation of the initial geometry, i.e., ε_n and Ψ_n, respectively, may result in such flow decorrelations [27–29]. Longitudinal decorrelations have been measured in nucleus-nucleus collisions and these effects are larger for v_3 compared to v_2 [30,31]. The decorrelations effects are found to be larger at lower collision energies [32,33], and have not been quantified in small system collisions, notably $p/d/^3$He +Au at RHIC. Since the PHENIX results have detectors covering a range of pseudorapidities, the detector

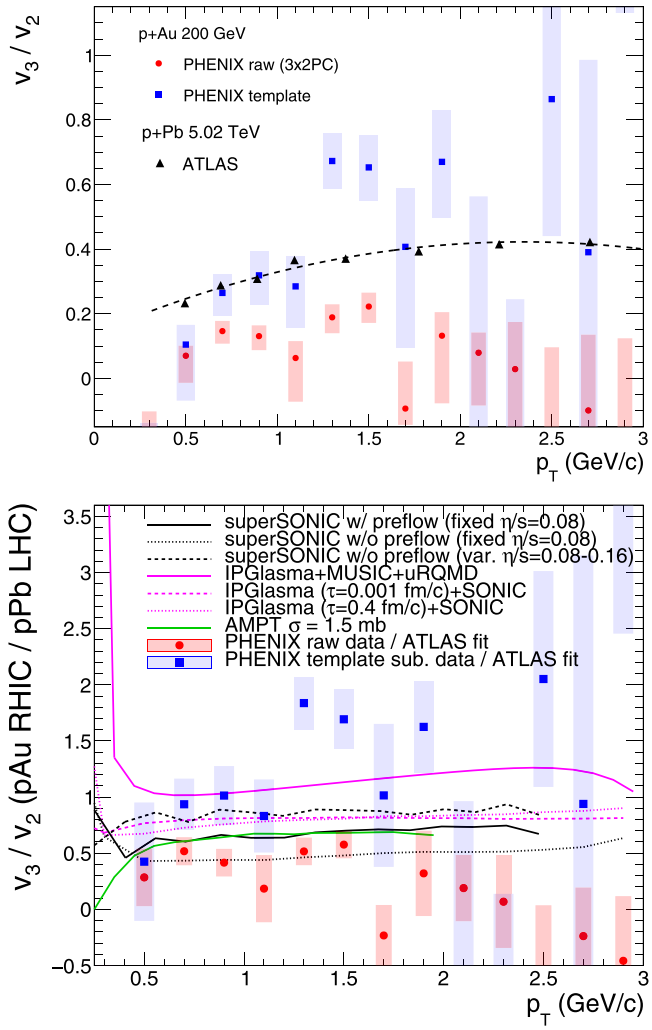

FIG. 12. (Upper) Ratio of v_3/v_2 as a function of p_T from ATLAS p+Pb collisions at $\sqrt{s_{NN}} = 5$ TeV and PHENIX raw and template adjusted p+Au collisions at $\sqrt{s_{NN}} = 200$ GeV. Uncertainties shown are statistical only. (Lower) Double ratio of PHENIX raw and template adjusted data over the ATLAS data fit compared with various theoretical calculations.

combinations used could be influenced by such decorrelations.

If we consider the parametrization of decorrelation used by the CMS Collaboration [31], the correlation coefficients can be written as $c_n = v_{n,a} \times v_{n,b} \times \exp[-\alpha\Delta\eta]$. In this case, the two-particle Fourier coefficient is now not simply the multiplicative product of the flow coefficient for particle a and particle b, but includes a longitudinal decorrelation proportional to the exponential of the pseudorapidity gap between particles a and b and a proportionality constant α. While it is unclear if this parametrization holds in $p/d/^3$He +Au collisions over a wide range in pseudorapidity, it is nonetheless useful to explore the implications. In the case of the BBCS-FVTXS-CNT detector combination, the $\Delta\eta$ values are approximately 3.5, 1.75, 1.75 for the BBCS-CNT, BBCS-FVTXS, FVTXS-CNT, respectively. One can express this

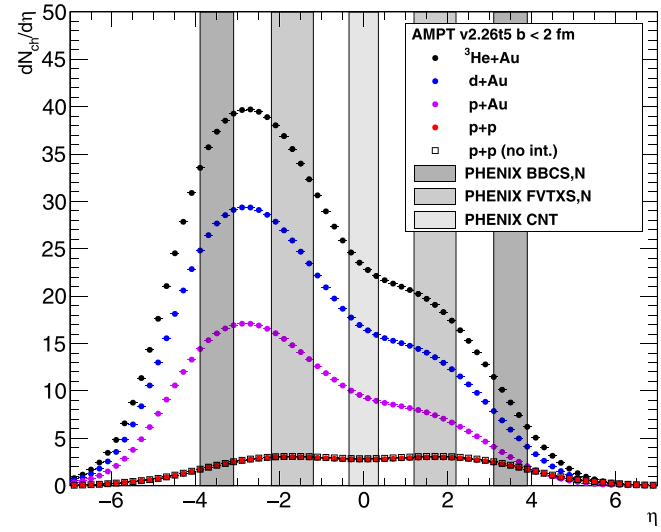

FIG. 13. Results from AMPT for $dN_{ch}/d\eta$ as a function of η in minimum bias p+p (with and without final-state interactions) and central ($b < 2$ fm) p+Au, d+Au, and ^{3}He +Au collisions at $\sqrt{s_{NN}} = 200$ GeV. Also highlighted are the approximate pseudorapidity acceptances for the PHENIX detector systems.

as below:

$$v_n(\mathrm{CNT}) = \sqrt{\frac{c_n[\mathrm{BBCS\text{-}CNT}] \times c_n[\mathrm{FVTXS\text{-}CNT}]}{c_n[\mathrm{BBCS\text{-}FVTXS}]}} \tag{8}$$

$$= \sqrt{\frac{v_n[\mathrm{BBC}]v_n[\mathrm{CNT}]e^{-3.5\alpha} \times v_n[\mathrm{FVTXS}]v_n[\mathrm{CNT}]e^{-1.75\alpha}}{v_n[\mathrm{BBCS}]v_n[\mathrm{FVTXS}]e^{-1.75\alpha}}} \tag{9}$$

$$= v_n[\mathrm{CNT}]e^{-3.5\alpha/2} \tag{10}$$

and one finds that in this case the decorrelation between the BBCS-FVTXS and FVTXS-CNT cancels, and only the

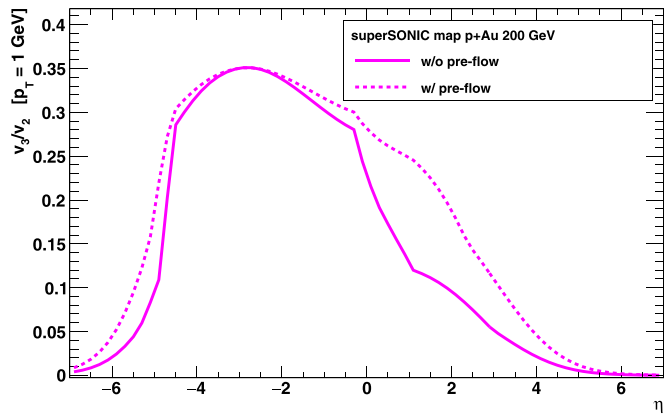

FIG. 14. Theoretical predictions for the ratio v_3/v_2 at $p_T = 1.0$ GeV as a function of pseudorapidity in p+Au collisions at $\sqrt{s_{NN}} = 200$ GeV. Results are shown for with (SUPERSONIC) and without (SONIC) strongly coupled preflow. See text for calculation details.

TABLE I. Summary of various initial geometry calculations quantified by the average eccentricities $\varepsilon_{2(3)}$ in central (impact parameter $b < 2$ fm) p+Au, d+Au, ^{3}He +Au events. The values quoted have statistical uncertainties of 0.01 or smaller. Column 2 uses Monte Carlo Glauber with nucleon position fluctuations [9]. Column 3 uses Monte Carlo Glauber with nucleon position fluctuations and negative binomial distribution (NBD) fluctuations in particle production [25]. Column 4 uses Monte Carlo Glauber with constituent quark position fluctuations and NBD fluctuations [25]. Columns 5 and 6 use the IP-GLASMA framework with nucleon and constituent quark position fluctuations respectively, where both include gluon field fluctuations [26]. These results were obtained with the publicly available IP-GLASMA code.[a]

Collision system	Nucl. without NBD fluc.	Nucl. without NBD fluc.	Quarks with NBD fluc.	IP-G with nucl.	IP-G with quarks
			$\langle\varepsilon_2\rangle$		
p+Au	0.23	0.32	0.38	0.10	0.50
d+Au	0.54	0.48	0.51	0.58	0.73
^{3}He +Au	0.50	0.50	0.52	0.55	0.64
			$\langle\varepsilon_3\rangle$		
p+Au	0.16	0.24	0.30	0.09	0.32
d+Au	0.18	0.28	0.31	0.28	0.40
^{3}He +Au	0.28	0.32	0.35	0.34	0.46

[a]The eccentricities from IP-GLASMA depend on where the Q_s^2 Gaussian distribution in transverse coordinates is truncated. For these values $r_{\max} = 3$ fm was utilized.

square root of the BBCS-CNT decorrelation remains. Thus, $\alpha = 0.054$ would correspond to a 10% decorrelation in c_n over a two-unit rapidity gap, corresponding to a 9% lower v_n being measured by the BBCS-FVTXS-CNT combination. In contrast, in the case of FVTXS-CNT-FVTXN, all of the decorrelation cancels out in that combination. Of course, this all assumes this simple exponential model. More detailed modeling of longitudinal decorrelation effects in small systems might lend more insights.

VIII. SUMMARY

Utilizing the PHENIX published correlation coefficients, we have tested various flow and nonflow adjustment methods. The results vary depending on the method quantitatively and we have discussed potential implications in light of significant nonclosure results with AMPT and PYTHIA/ANGANTYR. Comparisons between p+Au at RHIC and p+Pb at the LHC elucidate the potential influence of prehydrodynamic evolution, via comparisons with (SUPER)SONIC calculations. The conclusion that these flow coefficients are dominated by initial geometry coupled with final-state interactions (e.g., hydrodynamic expansion of quark-gluon plasma) is confirmed, and explanations based on initial-state glasma are ruled out. The detailed balance of intrinsic geometry and fluctuation-driven geometry as well as the exact role of weak or strong coupled prehydrodynamic evolution remain open questions requiring further theoretical and experimental investigation.

ACKNOWLEDGMENTS

We thank the PHENIX Collaboration for useful, open discussions and suggestions leading to this manuscript. We thank the Brookhaven National Laboratory Small System Task Force (Constantin Loizides, Jean-Yves Ollitrault, Sergei Voloshin) for useful input. We acknowledge useful discussions with Paul Romatschke, Julia Velkovska, and Bill Zajc. J.L.N. acknowledges support from the U.S. Department of Energy, Office of Science, Office of Nuclear Physics under Contract No. DE-FG02-00ER41152. S.H.L. acknowledges support from the National Research Foundation of Korea (NRF) grant funded by the Korea government (MSIT) under Contract No. 2020R1C1C1004985.

[1] U. Heinz and R. Snellings, Collective flow and viscosity in relativistic heavy-ion collisions, Annu. Rev. Nucl. Part. Sci. **63**, 123 (2013).
[2] P. Romatschke, Do nuclear collisions create a locally equilibrated quark–gluon plasma? Eur. Phys. J. C **77**, 21 (2017).
[3] M. P. Heller and M. Spalinski, Hydrodynamics Beyond the Gradient Expansion: Resurgence and Resummation, Phys. Rev. Lett. **115**, 072501 (2015).
[4] P. Romatschke and U. Romatschke, *Relativistic Fluid Dynamics In and Out of Equilibrium*, Cambridge Monographs on Mathematical Physics (Cambridge University Press, Cambridge, UK, 2019).
[5] G. Nijs, W. van der Schee, U. Gürsoy, and R. Snellings, Bayesian analysis of heavy ion collisions with the heavy ion computational framework Trajectum, Phys. Rev. C **103**, 054909 (2021).
[6] D. Everett, W. Ke, J. F. Paquet, G. Vujanovic, S. A. Bass, L. Du, C. Gale, M. Heffernan, U. Heinz, D. Liyanage, M. Luzum, A. Majumder, M. McNelis, C. Shen, Y. Xu, A. Angerami, S. Cao, Y. Chen, J. Coleman, L. Cunqueiro, T. Dai, R. Ehlers, H. Elfner, W. Fan, R. J. Fries, F. Garza, Y. He, B. V. Jacak, P. M. Jacobs, S. Jeon, B. Kim, M. Kordell, A. Kumar, S. Mak, J. Mulligan, C. Nattrass, D. Oliinychenko, C. Park, J. H. Putschke, G. Roland, B. Schenke, L. Schwiebert, A. Silva, C. Sirimanna, R. A. Soltz, Y. Tachibana, X. N. Wang, and R. L. Wolpert (JETSCAPE), Multisystem Bayesian constraints on the transport coefficients of QCD matter, Phys. Rev. C **103**, 054904 (2021).
[7] J. L. Nagle and W. A. Zajc, Small system collectivity in relativistic hadronic and nuclear collisions, Annu. Rev. Nucl. Part. Sci. **68**, 211 (2018).
[8] P. Romatschke, Light-heavy ion collisions: A window into preequilibrium QCD dynamics? Eur. Phys. J. C **75**, 305 (2015).
[9] J. L. Nagle, A. Adare, S. Beckman, T. Koblesky, J. O. Koop, D. McGlinchey, P. Romatschke, J. Carlson, J. E. Lynn, and M. McCumber, Exploiting Intrinsic Triangular Geometry in Relativistic He3+Au Collisions to Disentangle Medium Properties, Phys. Rev. Lett. **113**, 112301 (2014).
[10] C. Aidala *et al.* (PHENIX), Creation of quark–gluon plasma droplets with three distinct geometries, Nat. Phys. **15**, 214 (2019).

[11] U. A. Acharya *et al.* (PHENIX Collaboration), Kinematic dependence of azimuthal anisotropies in p+Au, d+Au, and ^{3}He + Au at $\sqrt{s_{NN}} = 200$ GeV, Phys. Rev. C **105**, 024901 (2022).

[12] M. Mace, V. V. Skokov, P. Tribedy, and R. Venugopalan, Hierarchy of Azimuthal Anisotropy Harmonics in Collisions of Small Systems From the Color Glass Condensate, Phys. Rev. Lett. **121**, 052301 (2018); **123**, 039901(E) (2019).

[13] M. Mace, V. V. Skokov, P. Tribedy, and R. Venugopalan, Systematics of azimuthal anisotropy harmonics in proton–nucleus collisions at the LHC from the color glass condensate, Phys. Lett. B **788**, 161 (2019); **799**, 135006(E) (2019).

[14] G. Aad *et al.* (ATLAS), Measurement of angular and momentum distributions of charged particles within and around jets in Pb+Pb and pp collisions at $\sqrt{s_{NN}} = 5.02$ TeV with the ATLAS detector, Phys. Rev. C **100**, 064901 (2019); **101**, 059903(E) (2020).

[15] A. Adare *et al.* (PHENIX), Dihadron azimuthal correlations in Au+Au collisions at $\sqrt{s_{NN}} = 200$ GeV, Phys. Rev. C **78**, 014901 (2008).

[16] G. Aad *et al.* (ATLAS), Measurement of long-range pseudorapidity correlations and azimuthal harmonics in $\sqrt{s_{NN}} = 5.02$ TeV proton-lead collisions with the ATLAS detector, Phys. Rev. C **90**, 044906 (2014).

[17] S. H. Lim, Q. Hu, R. Belmont, K. K. Hill, J. L. Nagle, and D. V. Perepelitsa, Examination of flow and nonflow factorization methods in small collision systems, Phys. Rev. C **100**, 024908 (2019).

[18] A. Adare *et al.* (PHENIX), Centrality categorization for $R_{p(d)+A}$ in high-energy collisions, Phys. Rev. C **90**, 034902 (2014).

[19] A. Adare *et al.* (PHENIX), Pseudorapidity Dependence of Particle Production and Elliptic Flow in Asymmetric Nuclear Collisions of p+Al, p+Au, d+Au, and ^{3}He +Au at $\sqrt{s_{NN}} =$ 200 GeV, Phys. Rev. Lett. **121**, 222301 (2018).

[20] Z.-W. Lin, C. M. Ko, B.-A. Li, B. Zhang, and S. Pal, A multiphase transport model for relativistic heavy ion collisions, Phys. Rev. C **72**, 064901 (2005).

[21] J. D. Orjuela Koop, A. Adare, D. McGlinchey, and J. L. Nagle, Azimuthal anisotropy relative to the participant plane from a multiphase transport model in central p+Au, d+Au, and ^{3}He +Au collisions at $\sqrt{s_{NN}} = 200$ GeV, Phys. Rev. C **92**, 054903 (2015).

[22] J. L. Nagle and J. Orjuela Koop, A quasiparticle transport explanation for collectivity in the smallest of collision systems (pp and $e + e-$), Nucl. Phys. A **982**, 455 (2019).

[23] C. Bierlich, G. Gustafson, L. Lönnblad, and H. Shah, The angantyr model for heavy-ion collisions in PYTHIA8, J. High Energy Phys. 10 (2018) 134.

[24] B. Schenke, C. Shen, and P. Tribedy, Running the gamut of high energy nuclear collisions, Phys. Rev. C **102**, 044905 (2020).

[25] K. Welsh, J. Singer, and U. W. Heinz, Initial state fluctuations in collisions between light and heavy ions, Phys. Rev. C **94**, 024919 (2016).

[26] B. Schenke, P. Tribedy, and R. Venugopalan, Fluctuating Glasma Initial Conditions and Flow in Heavy Ion Collisions, Phys. Rev. Lett. **108**, 252301 (2012).

[27] L.-G. Pang, G.-Y. Qin, V. Roy, X.-N. Wang, and G.-L. Ma, Longitudinal decorrelation of anisotropic flows in heavy-ion collisions at the CERN Large Hadron Collider, Phys. Rev. C **91**, 044904 (2015).

[28] P. Bożek and W. Broniowski, Longitudinal decorrelation measures of flow magnitude and event-plane angles in ultrarelativistic nuclear collisions, Phys. Rev. C **97**, 034913 (2018).

[29] A. Behera, M. Nie, and J. Jia, Longitudinal eccentricity decorrelations in heavy ion collisions, Phys. Rev. Research **2**, 023362 (2020).

[30] G. Aad *et al.* (ATLAS), Longitudinal Flow Decorrelations in Xe+Xe Collisions at $\sqrt{s_{\rm NN}} = 5.44$ TeV with the ATLAS Detector, Phys. Rev. Lett. **126**, 122301 (2021).

[31] V. Khachatryan *et al.* (CMS), Evidence for transverse momentum and pseudorapidity dependent event plane fluctuations in Pb-Pb and p-Pb collisions, Phys. Rev. C **92**, 034911 (2015).

[32] M. Nie (STAR), Energy dependence of longitudinal flow decorrelation from STAR, Nucl. Phys. A **1005**, 121783 (2021).

[33] C. Shen and B. Schenke, Dynamical initial-state model for relativistic heavy-ion collisions, Phys. Rev. C **97**, 024907 (2018).